Inorganic Chemistry

Article

pubs.acs.org/IC

# Oxidation and Oxygenation of Carbonyl Ruthenium(II) Azuliporphyrin

Michał J. Białek, Agata Białońska, and Lechosław Latos-Grażyński*

Department of Chemistry, University of Wrocław, F. Joliot-Curie 14, 50-383 Wrocław, Poland

Supporting Information

**ABSTRACT:** Chemical oxidation and oxygenation of carbonyl ruthenium(II) azuliporphyrin [Ru(TPAP)(CO)] were explored. [Ru(TPAP)(CO)] reacts with dioxygen giving carbonyl ruthenium(II) 21-oxyazuliporphyrin [Ru(TPAP-O)(CO)] revealing the activation the Ru−C bond inside azuliporphyrin coordination cavity. Solution and X-ray structural studies confirmed the tendency of [Ru(TPAP-O)(CO)] to form dimeric $[Ru(TPAP\text{-}O)(CO)]_2$. The dimer adopts a head-to-tail structure with the azulenolate groups forming bridges from one macrocycle to the ruthenium(II) in the adjacent unit. One-electron oxidation of [Ru(TPAP)(CO)] gives the first $\pi$-cation radical of metallocarbaporphyrinoid—$[Ru(TPAP)(CO)]^{+\bullet}$—with extraordinary participation of the azulene unit in the spin delocalization. The most characteristic $^1$H NMR features of the radical are large, sign-alternating isotropic shifts of resonances assigned to *meso*-aryl, azulene, and pyrrolic hydrogen atoms. The spin distribution determined by density functional theory confirmed the $\pi$-cation radical electronic structure reproducing the diagnostic spectroscopic features including $\pi$-delocalization at *meso*-aryl resonances and very characteristic sign alternation of contact shifts for an azulene moiety.

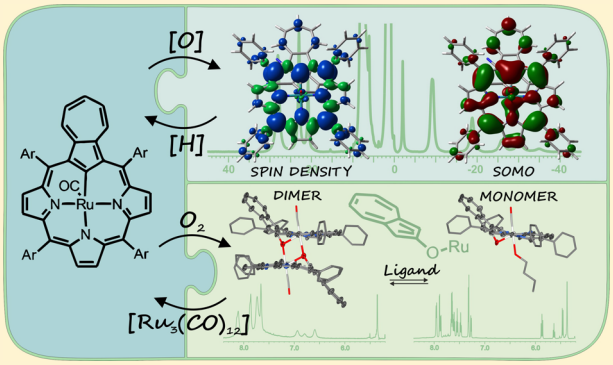


## INTRODUCTION

A dynamic development of synthetic routes of carbaporphyrinoids allows an exploration of a porphyrin-like or porphyrin-unlike coordination chemistry.[1−9] A set of organometallic derivatives formed by a combination of metal cations and appropriately tuned carbaporphyrinoids may serve as a perfect (chemically and structurally) environment to explore innovative organometallic chemistry in a "vessel" formed by porphyrin-like surrounding. The remarkable structural flexibility of carbaporphyrinoids, including N-confused porphyrin, is reflected by adaptation of various coordination modes inside a macrocyclic frame, with or without formation of a direct metal−carbon bond. Atypical oxidation states of metal ions can be trapped in organometallic settings,[2,4] for instance, extremely rare organocopper(II) complexes.[10−12]

Azuliporphyrin **1** is a member of the carbaporphyrinoid family with an azulene moiety built into the framework (Scheme 1).[13,14] The straightforward and facile synthetic route for 5,10,15,20-tetraarylazuliporphyrin (TArAP) is enabled by specific suitability of azulene as a substrate for Rothemund-type condensation.[14−17] Thus, this ligand can be considered as a highly attractive candidate for exploration of organometallic chemistry inside the carbaporphyrinoid core.[2] Till present, in contrast to flexible structures of other carbaporphyrinoids, *meso*-tetraaryl and $\beta$-alkylated azuliporphyrins form organometallic compounds where solely a direct M−C $\sigma$-bond [M = Ni(II), Pd(II), Pt(II), Ir(III)] has been detected.[4,18−20] Dithiaethyneazuliporphyrin, the contracted carbaporphyrinoid that contains an azulene moiety embedded in the [18]-dithiacarbatriphyrin(4.1.1) macrocyclic framework acted as a monoanionic ligand forming the Ru−C($sp^2$) $\sigma$-bond as well.[21] A different situation was observed when copper(II) acetate reacted with tetraarylazuliporphyrin **1** affording copper(II) complex of 21-hydroxyazuliporphyrin **1**−OH.[22] Recently we demonstrated that the azulene moiety can act as an independent coordination platform due to specific properties of its $\pi$-surface giving rise to a series of cluster complexes with general formula $[M(TPAP)\{Ru_4(CO)_9\}]$, in which M = Ru(CO), Ni, Pd, Pt.[23]

**Scheme 1. Azuliporphyrin and 21-Hydroxyazuliporphyrin**

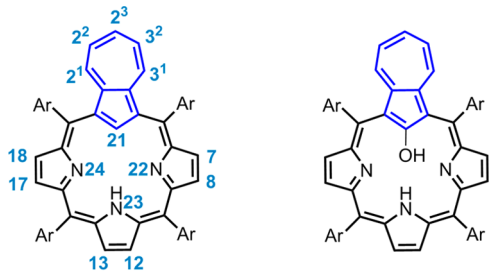


**Received:** February 10, 2015
**Published:** April 3, 2015





DOI: 10.1021/acs.inorgchem.5b00324
*Inorg. Chem.* 2015, 54, 6184−6194

**Scheme 2. Synthesis and Reactivity of Carbonyl Ruthenium(II) 21-Oxyazuliporphyrins 3 and 4**[a]

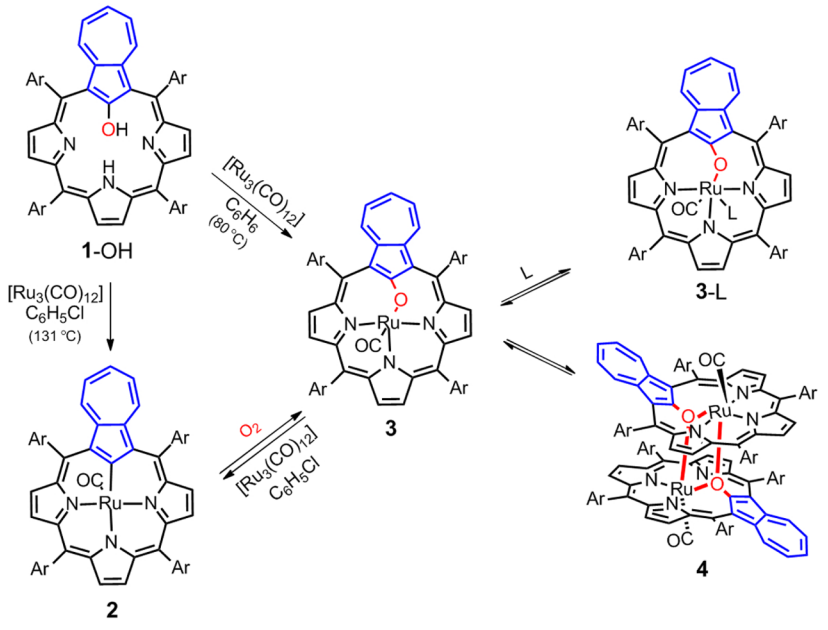


[a]Axial ligand L = $Et_3N$ (TEA), *n*-BuOH, Py-$d_5$.

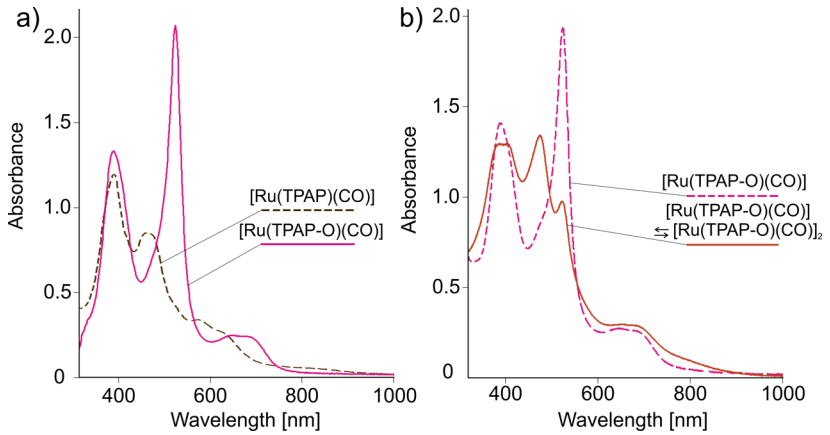


**Figure 1.** Electronic UV−vis spectra (chloroform 293 K) of (a) monomeric **2**-TEA (brown, dashed) and **3**-TEA (pink), (b) **3**-TEA in chloroform (pink, dashed), **3** and **4** (dimeric) in thermodynamic equilibrium **4** (red).

The present contribution concerns chemical oxidation and/or oxygenation of ruthenium(II) azuliporphyrin **2**—[Ru(TPAP)(CO)]. Activation of the Ru−C bond by molecular oxygen leads to the formation of complex **3**—[Ru(TPAP-O)(CO)]—showing a more general tendency in reactivity of the M−C bond inside an azuliporphyrin coordination cavity. One-electron oxidation of **2** gives the first $\pi$-cation radical of metallocarbaporphyrinoid **6** with extraordinary participation of the azulene unit in spin delocalization as showed by $^1$H NMR and theoretical investigations.

$^1$H NMR spectroscopy has been extensively applied to paramagnetic molecules including a variety of paramagnetic metalloporphyrins and metalloproteins.[6,24−27] Subsequently, this technique was also used to paramagnetic metallocarbaporphyrinoids incorporating copper(II), iron(II), iron(III), or nickel(II)[6,28−38] giving the fundamental spectroscopic comprehension of molecular and electronic structures, metal−arene interactions, structural rearrangements, and intramolecular reactivity. In this study, particular emphasis was put on $^1$H NMR studies as a source of insight into the electronic and molecular structures of oxidized ruthenium carbaporphyrinoids. These electronic structures can be compared to those of the related and much more intensively studied ruthenium regular porphyrins.[39−44]

## RESULTS AND DISCUSSION

**Synthesis and Spectroscopic Properties.** A ruthenium(II) ion was readily inserted into azuliporphyrin **1** in the reaction with a sub- or equimolar amount of $[Ru_3(CO)_{12}]$ affording carbonyl ruthenium(II) azuliporphyrin [Ru(TPAP)(CO)] **2** as reported previously.[23]

Solution of **2** undergoes very slow reaction with dioxygen at 298 K (Scheme 2, conversion of **2** to **3**). The reaction time can be significantly shortened in elevated temperature. The transformation of **2** involves an oxygenation at the C(21) position. This leads to a formation of carbonyl ruthenium(II) 21-oxyazuliporphyrin [Ru(TPAP-O)(CO)] (**3**) albeit in a relatively low yield suggesting stability of the Ru−C bond in


DOI: 10.1021/acs.inorgchem.5b00324
*Inorg. Chem.* 2015, 54, 6184−6194

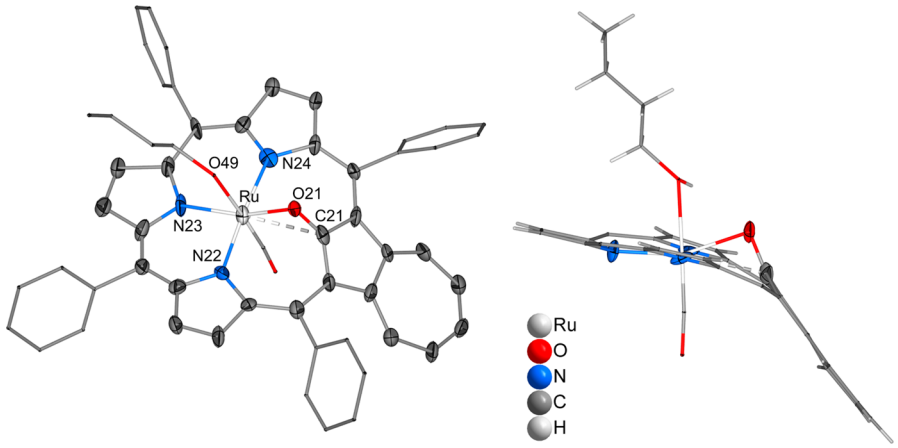


**Figure 2.** Molecular structure of **3**-$^{n}$BuOH (left, perspective view; right, presentation of macrocyclic folding with aryl groups omitted for clarity). The displacement ellipsoids represent 30% probability. Selected bond distances [Å]: Ru−N(22), 2.025(10); Ru−N(23), 2.024(10); Ru−N(24), 2.028(10); Ru−O(21) 2.072(8); Ru−O(49) 2.206(10); Ru−C(21), 2.523(13).

**2**. **3** is also a product of reaction of 21-hydroxyazuliporphyrin (**1**−OH) and triruthenium(0) dodecacarbonyl (conversion of **1**−OH to **3**). The reaction of [Ru(TPAP-O)(CO)] with $[Ru_3(CO)_{12}]$ in chlorobenzene recovers [Ru(TPAP)(CO)] (Scheme 2, conversion of **3** to **2**). The ruthenium(0) cluster seems to act as a reducing agent scavenging the 21-oxy bridge in the temperature of boiling chlorobenzene. Thus, the direct Ru−C bond is recovered. The same reactivity pattern is reproduced when 21-hydroxyazuliporphyrin **1**−OH reacts with ruthenium dodecacarbonyl in boiling chlorobenzene (conversion of **1**−OH to **2**).

The equatorial (CNNN) donor set of **2** was replaced by the (ONNN) one at the coordination crevice of **3**. [Ru(TPAP-O)(CO)] is stable and was purified by the standard chromatographic procedures. Subsequently, **3** has also been isolated in the solid state as the monomeric complex ligated with *n*-butanol—[Ru(TPAP-O)(CO)(*n*-butanol)] (**3**-$^{n}$BuOH) or as dimeric complex $[Ru(TPAP-O)(CO)]_2$ (**4**) depending on the way of crystallization.

The products **3**-L (L—axial ligand) and **4** (in equilibrium with **3**) were characterized in solution by $^{1}$H NMR and UV−vis spectroscopy. This characterization was supported by high-resolution mass spectrometry (HRMS). [Ru(TPAP-O)(CO)] ionizes in electrospray conditions to $[Ru(TPAP-O)(CO)]H^+$ and dimeric $[Ru(TPAP-O)(CO)]_2H^+$. Calcd for $C_{51}H_{32}N_3O_2Ru$ (M + H$^+$) (**3** + H$^+$): 820.1538; found: 820.1521; $C_{102}H_{63}N_6O_4Ru_2$ (M + H$^+$) (**4** + H$^+$): 1639.3036; found: 1639.3025 (*m*/*z*) with an isotopic distribution consistent with the chemical composition (Supporting Information, Figures S4 and S5).

When **2** is oxygenated to **3**, significant changes are readily detected in electronic spectra (Figure 1a). To facilitate the comparison the spectra were taken in the presence of triethylamine (TEA) acting as auxiliary ligand that occupies the axial position in **2**-TEA and **3**-TEA (Figure 1a, traces brown and pink, respectively). The noticeable increase of splitting of the most intense two bands was detected once the oxygen atom is inserted into the Ru−C(21) of **2** to form **3**. The markedly different spectrum for **3** was measured in chlorinated solvents in absence of additional ligands (Figure 1b, red trace). Such spectroscopic features were attributed to the thermodynamic equilibrium between **3** and its dimeric counterpart **4**. Evidently the apical coordination sites of two molecules of **3** were made available to mutual oxygen coordination allowing a head-to-tail dimerization yielding **4** (Scheme 2). Significantly the gradual decrease of dimer diagnostic band intensity (centered at 475 nm) parallel with increase of monomer diagnostic band intensity (centered at 524 nm) was detected following the temperature lowering.

The presence of carbonyl ligand in [Ru(TPAP-O)(CO)] was verified by infrared spectroscopy. The coordination of a carbonyl group for **3** was firmly confirmed by the characteristic frequency of the CO stretching, $\nu$(CO) = 1947 cm$^{-1}$, which is very close to that established for [Ru$^{II}$(TTP)(CO)(py)] and **2**.[23,45] The single CO resonance was detected at $^{13}$C NMR spectrum of **3**-py-$d_5$ (182.0 ppm, Supporting Information, Figure S1) with a position resembling those determined for carbonyl ruthenium(II) 5,10,15,20-tetraarylporphyrins[46,47] and **2**-py-$d_5$.[23]

**Molecular Structures of 3-$^{n}$BuOH and 4.** The molecular geometry of **3**-$^{n}$BuOH as determined by X-ray crystallography (Figure 2) reflects a balance between constraints of the macrocycle ligand, the size of the ruthenium(II) ion, and the predisposition of the ruthenium(II) ion for six-coordination in porphyrinic surroundings, resembling eventually some fundamental structural features of carbonyl ruthenium(II) porphyrin[46] or carbonyl ruthenium(II) azuliporphyrin.[23] The apical coordination sites are occupied by carbonyl and 1-butanol with the Ru−O distance of 2.206(10) Å. The Ru−O(21) distance is equal to 2.072(8) Å, and the Ru−C(21) distance equals 2.523(13) Å, which is only slightly longer than Cu−C(21) (2.474(3) Å) in analogous copper(II) complex [Cu(TPAP-O)].[22] The molecule demonstrates a deflection angle with the azulene that equals 52.1(4)° defined as the dihedral angle between a plane determined by azulene atoms and the $N_3$ plane. It is ca. 7° smaller than that found for [Cu(TPAP-O)].[22] The environment of C(21) is close to trigonal. The projection of the ruthenium(II) onto the C(21)−O bond lies close to oxygen atom as reflected by the Ru−O(21)−C(21) angle of 93.7(8)°.

The C(21)O(21) distance of 1.314(16) Å resembles these seen for nickel(II), iron(III), and rhodium(III) complexes of 21-hydroxy N-confused porphyrin[31,48−50] and is close to the C−O distance of 1.335 Å, which is typical for phenoxide ligands.[51]



DOI: 10.1021/acs.inorgchem.5b00324
*Inorg. Chem.* 2015, 54, 6184−6194

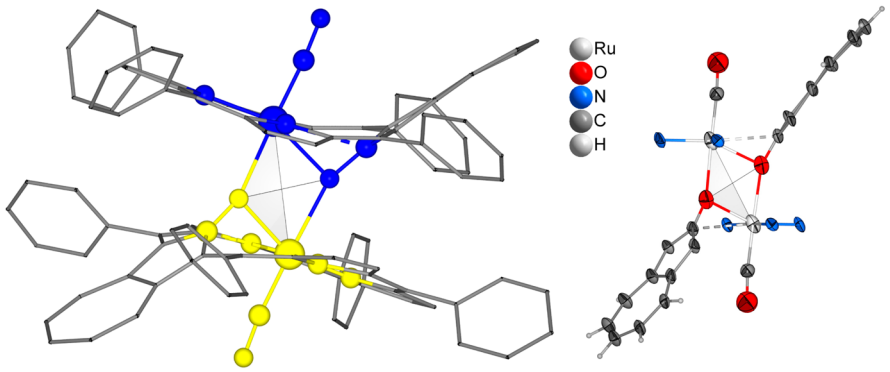


**Figure 3.** Molecular structure of **4** (left, perspective view with coordination centers marked with colors; right, a view showing an isolated diruthenium coordination center motif). The displacement ellipsoids represent 30% probability. Selected bond distances [Å]: Ru−N(22), 2.07(2); Ru−N(24), 2.015(19); Ru−O(21), 2.104(17); Ru−O(21)′, 2.235(17). A well-defined twist between subunits reflects the absence of the inversion center in **4**.

Structural studies confirmed the tendency of **3** to form a dimeric structure providing that potential ligands competing for apical position of ruthenium(II) are removed from solution. Thus, crystals of **4** grown by slow evaporation of dichloromethane solution were subjected to single-crystal X-ray diffraction (SC-XRD) measurements. Views of the dimeric molecule are shown in Figure 3. The dimer adopts a head-to-tail structure with the azulenolate groups forming bridges from one macrocycle to the ruthenium(II) in the adjacent unit. The Ru−Ru′ central ions are separated by 3.513(4) Å. The ruthenium(II) and oxygen atoms are located at the corners of deformed parallelogram defined by Ru, O(21), Ru′, and O(21′), in which the Ru−O(21)′−Ru′−O(21) torsion angle equals 13.9(8)°.

Both subunits are twisted with respect to each other as nicely reflected by the angle between axes determined by C(21)···N(23) and C(21)′···N(23)′ atoms that equals 23.3(9)° pointing for a non-centrosymmetric entity (symmetry of the selected crystal belongs to crystal space group $P4_32_12$). Each subunit consists of an approximately planar tripyrrolic fragment and a highly deflected azulene moiety ($N_3$ and C(1), C(2), C(3), C(4), C(21) planes; 53.6(10)°). The distance between the subunits measured as the distance between CNNN planes is close to 3.40 Å, which is also optimal for attractive stacking interactions. The bridging oxygen atom is bound to the second ruthenium center with the Ru−O distance equal to 2.235(17) Å, while the intramolecular Ru−O bond is 2.104(17) Å long.

**Nuclear Magnetic Resonance Studies.** The $^1$H NMR spectrum of tripyrrolic unit of **3**-py-$d_5$ resembles the basic pattern of 21-hydroxyazuliporphyrin consistent with the borderline macrocyclic aromaticity (Figure 4c). The spectrum contains an AB spin system at $\delta$ = 7.85, H(7,18), and $\delta$ = 7.27 ppm, H(8,17), with a coupling constant ($^3J$ = 5.1 Hz) typical for a pyrrole ring in porphyrinoids, which is accompanied by singlet at $\delta$ = 7.27 ppm, of central pyrrole unit H(12,13). The $^1$H and $^{13}$C resonances of azulene were assigned as follows: $^1$H NMR H($2^1$,$3^1$) 5.41, H($2^2$,$3^2$) 5.82, H($2^3$) 5.58 ppm; $^{13}$C NMR C($2^1$,$3^1$) 129.6, C($2^2$,$3^2$) 136.6, C($2^3$), 128.9 ppm.

In contrast to **3**-py-$d_5$ the visible broadening of all resonances was detected at 300 K for **3** (Figure 4b). These spectroscopic features are preserved in the whole investigated 190−300 K temperature range. With temperature change a smooth shift of the resonances can be also observed. It is clearly reflected by diagnostic azulene resonances, which relocated from 6.6 to 6.4 ppm (300 K) to 6.0−5.4 ppm (190 K) positions. Thus, $^1$H

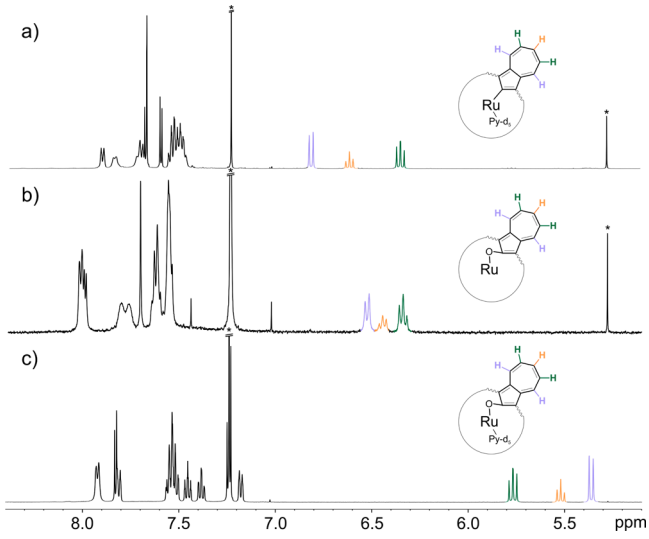


**Figure 4.** $^1$H NMR spectra (500 MHz, $CDCl_3$, 300 K) of (a) **2**-py-$d_5$, (b) cyclic **4** and acyclic dimers **5** in equilibrium with **3**, and (c) **3**-py-$d_5$.

NMR studies compelled consideration of the complex dynamic behavior that involves the thermodynamic equilibrium between monomeric **3** and acyclic (**5**-45 and **5**-135) and cyclic (**4**-1 and **4**-2) dimers (Scheme 3).

The effect of dimeric coordination upon the chemical shifts and line widths is certainly quite complex. The variable-temperature $^1$H NMR studies (Supporting Information, Figure S3) allowed elucidation of the conformational rearrangement of the acyclic dimer **5** engaging the intramolecular rotation of two subunits with respect to a single Ru−O(21)′ bridging bond. Accordingly an exchange, involving the cyclic dimeric **4**, a variety of acyclic dimeric rotamers, and monomeric **3**, is in limits to allow averaging of chemical shift. At the same time it is sufficiently slow to reveal features of intermediate exchange rates as far as increased line width is concerned.

Alternatively, an intramolecular enantiomerization can be invoked. In principle **4** adopts two enantiomeric conformations differentiated by puckering of Ru−O(21)−Ru′−O(21)′ parallelogram as discussed above in course of X-ray analysis (Figure 3). One can presume that the nonplanar arrangement of this structurally crucial ring is not very rigid. Thus, the dimer flips from one enantiomer (**4**-1) to another (**4**-2) via a unique


DOI: 10.1021/acs.inorgchem.5b00324
*Inorg. Chem.* 2015, 54, 6184−6194

**Scheme 3. Proposed Equilibria between 3, 4, and 5**

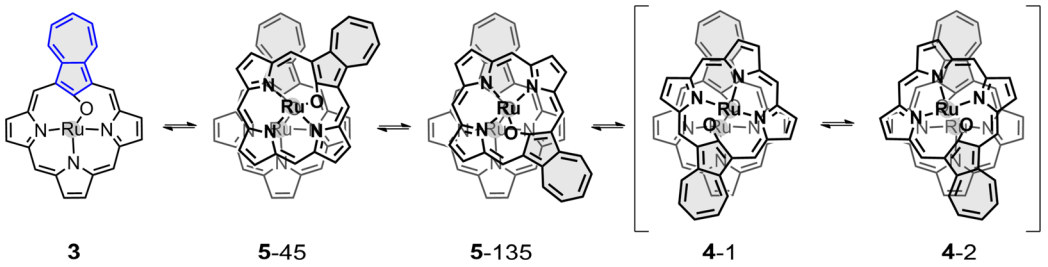


transformation (Figure 5), which seems consistent with $^1$H NMR data.

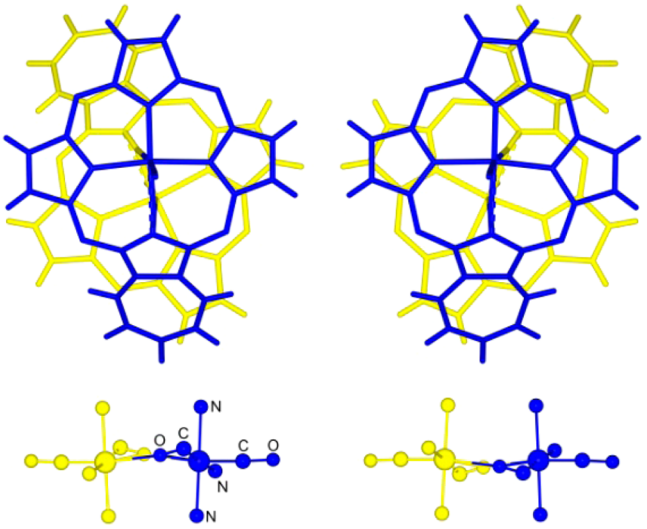

**Figure 5.** Top view of two enantiomers of **4** (one artificially generated from the X-ray data) showing the twisted conformation. The flip of the Ru−O(21)−Ru′−O(21)′ tetragon shown at the bottom view.

**Electrochemical Oxidation.** Cyclic voltammetry (Supporting Information, Figure S9) demonstrates that **2** undergoes two consecutive, reversible one-electron oxidations with semireversible half-wave potentials at (1) −0.048 V and (2) 0.42 V (dichloromethane, tetrabutylammonium perchlorate (TBAP), relative to the ferrocenium/ferrocene ($Fc^+$/Fc) couple). The first potential is relatively low, which accounts for the easy accessibility of an one-electron oxidized form. Similar values of oxidation potentials were determined for **3** ($E_{1/2}(1)$ = 0.04 V, $E_{1/2}(2)$ = 0.34 V). The oxidation potentials previously reported for palladium(II) azuliporphyrin, $E_{1/2}(1)$ = 0.46 (−0.06) V and $E_{1/2}(2)$ = 1.01 (0.49) V, versus Ag/$AgNO_3$ (values relative to the $Fc^+$/Fc couple in brackets) are in the same range as determined for **2**. Two subsequent one-electron ligand-centered processes in [Pd(TPAP)] were accounted for in this oxidation wave observation.[19] Considering the essential similarities in the oxidation patterns of ruthenium(II) and palladium(II) azuliporphyrins, one can suggest that the first one-electron oxidation of **2** is also ligand-centered yielding carbonyl ruthenium(II) azuliporphyrin $\pi$-cation radical **6**, and for **3** it is carbonyl ruthenium(II) 21-oxyazuliporphyrin $\pi$-cation radical **7**. Significantly, it is well-documented that the carbonyl complexes of ruthenium(II) regular porphyrin electrochemically or chemically undergo ring oxidation to form the $\pi$-cation radicals.[52−59]

**Chemical Oxidation of 2 and 3.** Oxidation of [Ru(TPAP)(CO)] (**2**) solutions in chloroform-*d* with varying amounts of 2,3-dichloro-5,6-dicyano-*p*-benzoquinone (DDQ) at 300 K was systematically followed by $^1$H NMR. Oxidation of **2** affords ruthenium(II) azuliporphyrin $\pi$-cation radical **6** (Scheme 4), which is persistent enough to be characterized in detail by UV−vis, IR, $^1$H NMR, and $^2$H NMR spectroscopies (Figure 6).

**Scheme 4. Chemical Oxidation of 2 to 6**

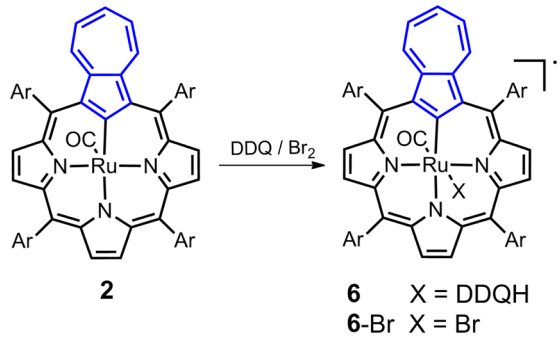


The addition of DDQ is accompanied by the loss of the $^1$H NMR resonances of **2** and the growth of resonances due to generation of **6**. The results of the complete one-electron oxidation are given in Figure 6c. Reduction of the **6** solution (e.g., with zinc dust) restores the $^1$H NMR spectrum of diamagnetic **2**.

The spectrum of **6**, shown in Figure 6, was collected at 270 K to achieve optimal resolution of broad resonances (linewidths vary in the 130−1170 Hz limits). An electron exchange between **2** and **6** is slow on the $^1$H NMR time scale at the whole investigated temperature range as the separate set of **2** and **6** resonances could be simultaneously detected after addition of substoichiometric amount of oxidant. The assignments, which are given above selected peaks (Figure 6c), were made on the basis of paramagnetic shifts, site-specific deuteration, and specific substitution of *meso*-aryls (Supporting Information, Figure S2). To identify pyrrole resonances, the $^1$H NMR spectrum of deuterated analogue **2**($d_x$) (deuterated at $\beta$-pyrrole positions with 85% efficiency) was synthesized and subsequently converted into **6**($d_x$). The appropriate $^1$H NMR spectrum of **6**($d_x$) revealed the significant decrease of intensity of pyrrole resonances (Figure S2). The complementary $^2$H NMR spectrum of **6**($d_x$) confirmed an assignment (Figure 6, inset). The chemical shifts and isotropic shifts are reported in Table 1.

The UV−vis electronic spectrum of **6** (Supporting Information, Figure S8) presents the broad features slightly bathochromically shifted in comparison to **2**. The coordination



DOI: 10.1021/acs.inorgchem.5b00324
*Inorg. Chem.* 2015, 54, 6184−6194

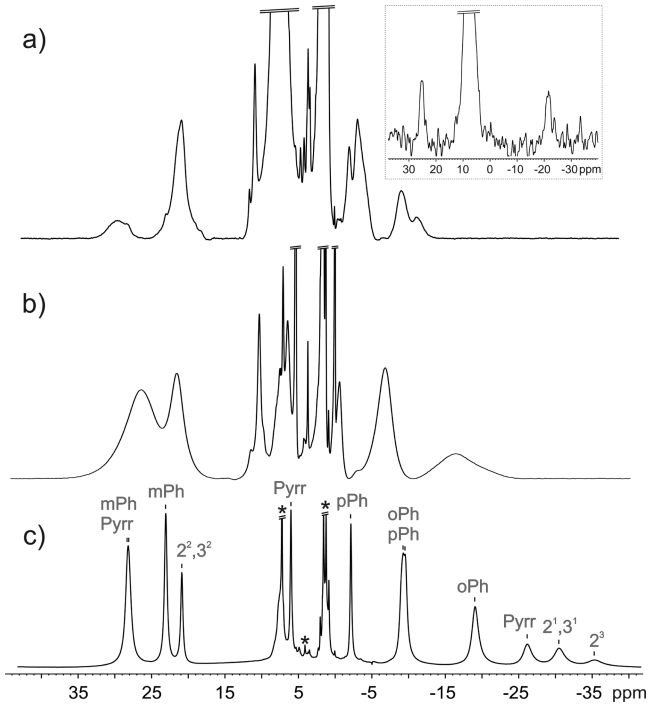


**Figure 6.** $^1$H NMR spectra ($CDCl_3$, 600 MHz, 270 K) generated by oxidation of (a) **3** to **7** with DDQ, (b) **2** to **6**-Br with $Br_2$, and (c) **2** to **6** with DDQ. (inset) The 92.12 MHz $^2$H NMR spectrum of **6**($d_x$) ($CHCl_3$/$CDCl_3$, 300 K).

of carbonyl in **6** was confirmed by the characteristic frequency of the CO stretching $\nu_{(CO)}$ = 1966 cm$^{-1}$, which is noticeably larger than that established for **2** ($\nu_{(CO)}$ = 1923 cm$^{-1}$). This change parallels results reported for oxidation of carbonyl ruthenium(II) porphyrin to carbonyl ruthenium porphyrin $\pi$-cation radical. In those studies the position of the diagnostic CO stretching band was shifted to higher values (due to oxidation of macrocycle one-electron) by 15−42 cm$^{-1}$ depending on choice of porphyrin (TPP or OEP), solvent and axial ligand.[58,59] The electron paramagnetic resonance (EPR) spectrum of **6** ($g$ = 2.01, toluene, 77 K) displays a pattern that suggests an electronic structure with a dominating cation radical contribution (Supporting Information, Figure S10).[61]

One-electron oxidation of **2** was also accomplished using $Br_2$ as an oxidizing agent (Figure 6b). The spectroscopic pattern of **6**-Br resembles that of **6** although all linewidths have considerably increased varying in the 360−1620 Hz limits. The high linewidths of the overlapping resonances precluded the detailed spectroscopic analysis for **6**-Br. The spectroscopic features of **6** differ from these of **6**-Br; thus, evidently different sixth (axial) ligands are coordinated after oxidations (for **6** presumably phenoxide is generated from DDQ, for **6**-Br bromide).

A Curie plot for the azulene, pyrrole, and *meso*-aryl resonances of **6** is given in Figure 7. The experimental data are consistent with linear behavior over the whole temperature range. The extrapolated intercepts are near the normal diamagnetic positions for diamagnetic [Ru(TPAP)(CO)] **2**.

**Table 1. $^1$H NMR Data for Paramagnetic Ruthenium Porphyrin and Ruthenium Porphyrinoids**

| ruthenium porphyrin | Pyrr | oPh | mPh | pPh | $2^1,3^1$ | $2^2,3^2$ | $2^3$ |
|---|---|---|---|---|---|---|---|
| **6**(diMeO)[a] | 27.8 | −4.2 | | −0.6 | −30.5 | 21.1 | −35.8 |
| | 6.6 | −4.8 | | −6.9 | | | |
| | −25.1 | | | | | | |
| **6**(Cl)[a] | 27.4 | −8.5 | 27.4 | | −29.3 | 20.5 | −33.8 |
| | 5.6 | −18.4 | 22.4 | | | | |
| | −26.1 | | | | | | |
| **6**(Me)[a] | 27.8 | −10.7 | 29.0 | (24.0) | −29.3 | 20.5 | −33.8 |
| | 6.3 | −21.0 | 23.7 | | | | |
| | −23.3 | | | (15.3) | | | |
| **6**[a] | 28.2 | −9.4 | 28.2 | −2.1 | −30.5 | 20.9 | −35.4 |
| | 6.0 | −19.1 | 23.1 | −9.4 | | | |
| | −26.2 | | | | | | |
| **6** isotropic shift[a,b] | 20.5 | −17.1 | 20.6 | −16.9 | −37.3 | 14.5 | −42.0 |
| | −1.7 | −26.8 | 15.5 | −9.6 | | | |
| | −33.9 | | | | | | |
| $\mathbf{6}_o$ calcd contact shift[a] | 42.7 | −41.3 | 17.6 | −36.9 | −37.1 | 11.5 | −37.8 |
| | 14.2 | −24.3 | 9.3 | −19.3 | | | |
| | −38.0 | | | | | | |
| $\mathbf{6}_o$-Br calcd contact shift[a] | 42.8 | −18.7 | 4.2 | −8.5 | −55.6 | 20.2 | −57.8 |
| | 16.8 | −21.5 | 7.5 | −15.7 | | | |
| | −26.9 | | | | | | |
| [$Ru^{II}$(TPP)Br(CO)]$^{\bullet}$[c,54] | 3.35 | −13.4 | 23.4 | −6.0 | | | |
| [$Ru^{II}$(TPP)Br(CS)]$^{\bullet}$[c,55] | −5.35 | −15.8 | 25.7 | 22.6 | | | |
| [$Ru^{III}$(TPP)Ph][d,60] | −30.9 | 2.6 | 4.5 | 5.5 | | | |
| | | 4.6 | 4.9 | | | | |
| [$Ru^{III}$(TPP)$(RNC)_2$]$(ClO_4)$[e,f,57] | 2.55 | −10.7 | 21.5 | −4.63 | | | |
| [$Ru^{IV}$(TPP)$Br_2$][d,60] | −48.0 | 5.2 | 12.8 | 5.8 | | | |

[a]270 K. [b]**2** as the diamagnetic reference. Descriptors in brackets for complex **6**, that is, diMeO, Cl, and Me, denote *meso*-phenyl substitution (3,5-dimethoxy, *p*-chloro, *p*-methyl (*p*-tolyl), respectively). [c]302 K. [d]300 K. [e]298 K. [f]R = 2,6-xylyl.



DOI: 10.1021/acs.inorgchem.5b00324
*Inorg. Chem.* 2015, 54, 6184−6194

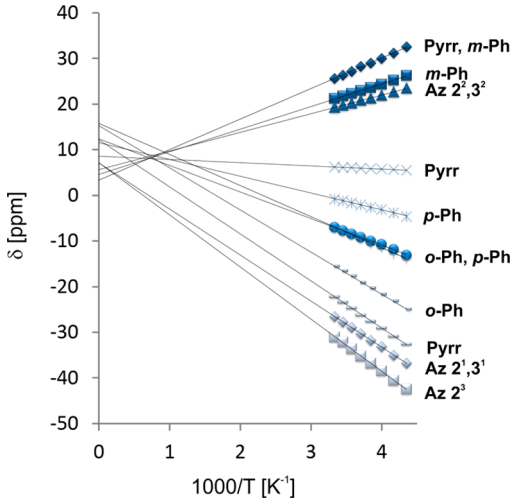


**Figure 7.** Curie plots for the azulene, pyrrole, and *meso*-aryl $^1$H NMR resonances of **6** ($CDCl_3$).

In the same manner as for **2** chemical oxidation of **3** was tested using DDQ and $Br_2$ as oxidants. Under the standard conditions the one-electron oxidation product **7**, observed solely when DDQ was used, exhibited very limited stability, and consequently the observations were limited to lower temperature to retard the rate of the product decay still achieving the reasonable spectroscopic features (Figure 6a). In such conditions formed species **7** survived for a short period of time, yet sufficient to collect a reasonable $^1$H NMR spectrum. The spectroscopic features of **7** resemble those of **6** albeit the spread of paramagnetically shifted resonances is smaller.

**Electronic Structure of 6.** One-electron oxidation of ruthenium(II) regular porphyrins may afford in principle three types of electronic structures.[52−57,60] Metal-centered oxidation yields ruthenium(III) regular porphyrin. Depending on a choice of axial ligand(s), two fundamental $(d_{xy})^2(d_{xz}d_{yz})^3$ or less-common $(d_{xy})^1(d_{xz}d_{yz})^4$ electronic structures were identified, which are differentiated by distribution of an unpaired electron on d-orbitals. Noticeably, an oxidation of carbonyl or thiocarbonyl ruthenium(II) regular porphyrins occurs preferentially at the porphyrinic ring to give an $a_{2u}$-cation radical species albeit the contribution of an alternative a1u-cation structure to a ground electronic state can be considered.[52−56] $^1$H NMR spectroscopy was shown to be a uniquely definitive method for detecting and characterizing paramagnetic metalloporphyrinoids.[24,27,62] The hyperfine shift patterns are sensitive to the oxidation, spin, and ligation states and allow addressing fine details of the electronic structure. The characteristic shifts for representative examples of paramagnetic ruthenium *meso*-tetraarylporphyrins derivatives are gathered in Table 1. The diagnostic spectrum pattern of carbonyl ruthenium(II) porphyrin $\pi$-cation radical, $[Ru^{II}(TPP)Br(CO)]^{\bullet}$, follows the spin distribution expected for the $a_{2u}$ electronic configuration (Table 1). Alternatively, ruthenium(III) porphyrin, $[Ru^{III}(TPP)(RNC)_2]ClO_4$, with a less common electronic ground state, demonstrated peculiar spin density distribution due to the partial delocalization of the $(d_{xy})^1$ unpaired electron into the $a_{2u}$ orbital of the porphyrin ring. It could be made possible by appropriate deformation of the porphyrin ring.[24,63−65] In such a case the porphyrin ring acquires also significant $a_{2u}$-type radical character due to the strong $a_{2u}-d_{xy}$ interaction.[24,63−65] Analysis of the data reveals that the specific feature of $a_{2u}$ porphyrin $\pi$-cation radicals is the distribution of a substantial amount of positive spin density at the meso carbon and pyrrole nitrogen atoms, while the $a_{1u}$ radical has a node at the meso positions but a large spin density at the pyrrole carbon atoms.[24,27] A correlation exists between the sign of the spin density on the meso carbon atom and the relative phenyl ring spectrum pattern.[24] In the case of the positive spin density, the phenyl ring shows an upfield shift for ortho and para and the downfield shift for meta resonances when the $\pi$-delocalization dominates the isotropic shift.

The interest in the one-electron oxidation product of ruthenium carbonyl 5,10,15,20-tetraarylazuliporphyrin **2** arises from spectroscopic and theoretical considerations regarding the electronic properties of ruthenium carbaporphyrinoid complexes. In comparison to ruthenium porphyrins with symmetrical peripheral substitution, the $^1$H NMR spectrum of **6** (Figure 6c, Table 1) is inherently more complex because of the reduction in symmetry from $C_{4v}$ to $C_s$, which occurs upon azulene incorporation. This overall mechanism of spin-density delocalization is expected to be more complex due to an extension of $\pi$-system by fusion of the tropylium ring. The most characteristic $^1$H NMR spectroscopic features of **6** are large, sign-alternating isotropic shifts of the *meso*-phenyl protons. The contact shift sign reversal after the *p*-methyl substitution of *meso*-phenyl is also consistent with the $\pi$-delocalization mechanism. The hyperfine shift pattern for the *meso*-aryls of **6** bears the essential resemblance to ruthenium(II) carbonyl *meso*-tetraarylporphyrins $\pi$-cation radicals considering both values and alternation of the isotropic shifts (Table 1). Importantly, the azulene resonances also demonstrate the diagnostic alternation of their isotropic shifts signs. The peculiar upfield and downfield spread of $\beta$-hydrogen resonances were recognized as well. These patterns of isotropic shifts features remain unprecedented in a group of paramagnetic ruthenium(III) porphyrins or ruthenium(II) porphyrins $\pi$-cation radicals.

**Electronic Structure—Density Functional Theory Calculations.** To assess the electronic structure of **6**, density functional theory (DFT) calculations were performed. The appropriate models of **2** and **3**, **6** and **7** were subjected to a DFT optimization at the B3LYP/6-31G(d,p)/LANL2DZ level of theory (Figures S11−S15). The final geometry corresponding to a one-electron oxidized derivative of carbonyl ruthenium azuliporphyrin **6** is shown in Figure 8.

One-electron oxidation preserves the essential geometric metrics of $\mathbf{2}_o$. In particular the bond lengths in the coordination core are only modestly changed (for $\mathbf{2}_o$: Ru−C(21) 2.020, Ru−N(22) 2.090, Ru−N(23) 2.136, Ru−N(24) 2.090 Å; for $\mathbf{6}_o$:

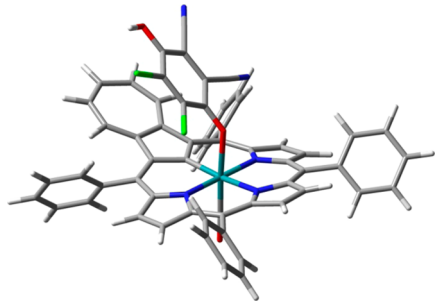

**Figure 8.** DFT-optimized structure of $\mathbf{6}_o$. The apical position occupied by a phenoxide derivative of DDQ.



DOI: 10.1021/acs.inorgchem.5b00324
*Inorg. Chem.* 2015, 54, 6184−6194

Ru−C(21) 2.001, Ru−N(22) 2.079, Ru−N(23) 2.144, Ru−N(24) 2.087 Å). The optimized structure $\mathbf{6}_o$ reveals the saddled conformation of the porphyrinic core. The metal ions are located in the plane defined by equatorial donor atoms (CNNN).

Figure 9 presents a diagram of selected molecular orbitals for $\mathbf{6}_o$. The electronic structure of $\mathbf{6}_o$ corresponds to the classical

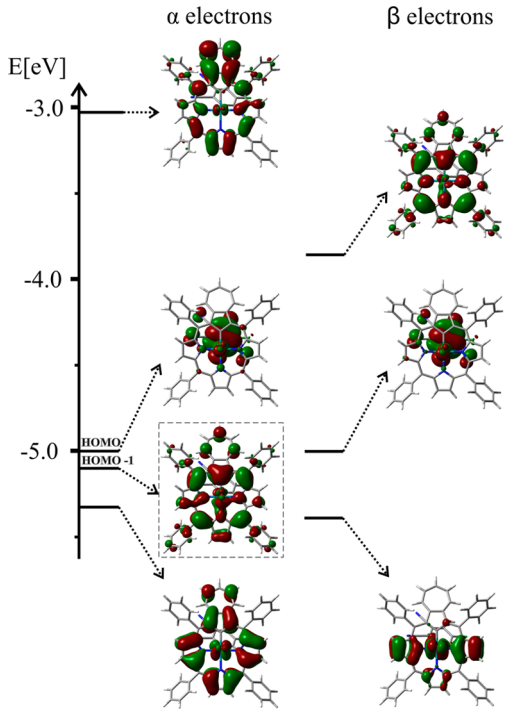


**Figure 9.** Diagram of selected energy levels and relevant molecular orbitals of complex $\mathbf{6}_o$ for $\alpha$ and $\beta$ electrons separately. All surfaces mapped with an isovalue of 0.02 and positive maxima marked red. The SOMO is put in a frame.

description of ruthenium(II) azuliporphyrin $\pi$-cation radical structure with a $(d_{xy})^2(d_{xz})^2(d_{yz})^2$ electronic configuration of the ruthenium(II) and the $\pi$-radical on the porphyrin.

The representative contour plots of the highest occupied molecular orbitals (HOMOs) for **6** are shown in Figure 9. In $\mathbf{6}_o$ the HOMO covers mainly DDQH axial ligand. The HOMO−1 is energetically very close to the HOMO and corresponds to the singly occupied molecular orbital (SOMO). It shows significant resemblance to the features of the total spin-density distribution (Figure 10) and the $a_{2u}$ orbital in $D_{4h}$ symmetry of regular porphyrins, which is quite typical for metalloporphyrin radicals.[24,66−68] That is, the large amplitudes at the meso positions and nitrogen atoms are preserved. In contrast to $a_{2u}$ of regular porphyrins the large amplitudes are detected at pyrrolic $\beta$-carbons. The incorporated azulene lowers the overall symmetry and contributes in a marked degree in composition of the orbital. The replacement of DDQH ligand by bromide ($\mathbf{6}_o$-Br) removes additional DDQ $\pi$-orbitals contribution producing the SOMO as the HOMO (Supporting Information, Figure S17). To facilitate the analysis the information on the spin-density distribution is presented in the form of plots of the surface of the total spin density (Figure 10).

Thus, the largest positive atomic spin density was determined at the meso, azulene, and some pyrrole positions. Importantly, the relatively small atomic spin density at the ruthenium ion

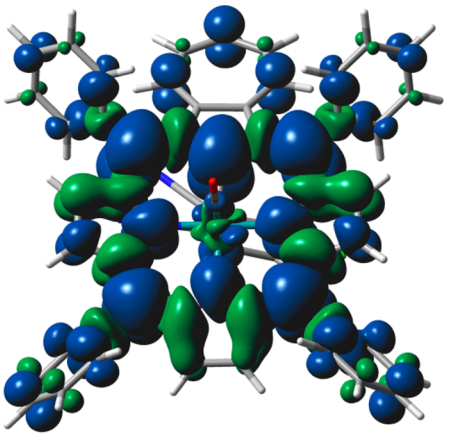

**Figure 10.** Plot of the total spin-density surface with isovalue = 0.0004 and the positive total density marked blue.

(−0.006), which is well below the density of ca. 1 expected presuming the $Ru^{III}$ $d^5$ electronic structure, is consistent with the ruthenium(II) $d^6$ $\pi$-cation radical description. The similar range of values typical for one-electron oxidation of a macrocycle were determined for metalloporphyrin $\pi$-cation radical[67,68] or metalloxoplorin radicals[69] containing metal ions that are redox innocent. The regular signs alteration of the spin density for azulene ($C2^1$ +, $C2^2$ −, $C2^3$ +) and the $\beta$-carbon atoms of the pyrrole ring adjacent to azulene (C7 −, C8 +) were successfully reproduced in DFT calculations. Calculations for $\mathbf{7}_o$ at the same level of theory give the same picture for 21-oxy derivative, albeit locating higher spin-density amplitudes at azulene carbon atoms.

Spin densities determined in the course of DFT studies on organic radicals are typically compared with experimental values—isotropic hyperfine coupling constants $a_N$ and contact shifts obtained from EPR and NMR spectroscopic measurements.[24] The spin density on carbon atoms (Supporting Information, Figures S16 and S18) can be converted into the isotropic shifts of attached protons. The detailed discussion of the methodology was given previously.[69−71] The comparison of experimental and theoretical spectra was schematically presented in Figure 11. An analysis leads to the fundamental conclusion that the spin distribution of **6** is reasonably well-accounted for by the ruthenium porphyrin $\pi$-cation radical structure. It is important to emphasize that DFT calculations reproduced qualitatively the following spectroscopic features: large $\pi$-delocalization at *meso*-aryl resonances, as well the sign

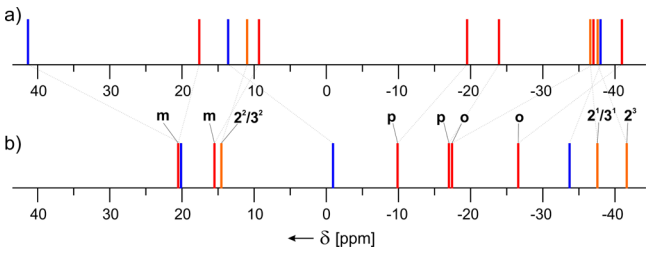


**Figure 11.** Schematic representation of (a) the experimental paramagnetic and (b) calculated contact shift patterns ($^1$H NMR) for **6**. Resonances labeling for azulene follows that given at Scheme 1. Applied code of colors: blue−pyrrole, orange−azulene, red—*meso*-aryl.



DOI: 10.1021/acs.inorgchem.5b00324
*Inorg. Chem.* 2015, 54, 6184−6194

alternation of contact shifts for azulene and adjacent pyrrole rings.

## CONCLUSIONS

Coordination chemistry of carbaporphyrinoids has typically revolved around the ability of these macrocycles to accommodate the metal cation of interest in the macrocyclic crevice. In this contribution we have demonstrated specific reactivity of carbonyl ruthenium(II) azuliporphyrin **2**. This complex undergoes one-electron oxidation to form ruthenium azuliporphyrin $\pi$-cation radical **6** with high participation of the azulene moiety in the spin delocalization. Complex **2** is reactive toward molecular oxygen providing new species **3** and **4** with an oxygen atom inserted to the Ru−C bond. Monomeric and dimeric complexes remain in thermodynamic equilibrium as long as the auxiliary ligand is absent in the solution.

No direct evidence for the formation of intermediates in the oxygenation process was found. An oxygenation mechanism can be considered as the insertion of a dioxygen molecule into the Ru−C bond to form a transient Ru−O−O−C(21) peroxide. A rapid O−O bond cleavage results in a unique situation in which two reactive centers are locked in the macrocyclic cage as a consequence of restraints imposed by the ligand structure. Further investigations of the ruthenium carbaporphyrinoid complexes are expected to afford an insight into the reactivity of a metal−carbon bond as specifically tuned carbaporphyrins can be expected to stabilize intermediates of the oxygenation process.

The field has the potential to produce ruthenium carbaporphyrinoids with chemical properties very different from those of regular ruthenium porphyrins[39,41−44,72−75] and the second relevant reference point−organometallic ruthenium pincer ligand complexes,[76−79] presuming that the equatorial macrocyclic ligand accepts an active organometallic role.

## EXPERIMENTAL SECTION

**Materials.** Chemicals and solvents like benzene, chlorobenzene, hexane isomers, etc., were at least pure grade and used without purification unless otherwise specified. Dichloromethane (DCM) was distilled over $CaH_2$.

**Carbonyl Ruthenium(II) 5,10,15,20-tetraarylazuliporphyrins [Ru(TArAP)(CO)] [2(*x*)].** (Ar = phenyl (**2**), *p*-tolyl [**2**(Me)], *p*-chlorophenyl [**2**(Cl)], 3,5-dimethoxyphenyl [**2**(diMeO)] or carbonyl ruthenium(II) 5,10,15,20-tetraphenylazuliporphyrin-$d_x$ [**2**($d_x$)] were prepared, as described elsewhere,[23] starting from appropriate 5,10,15,20-tetrarylazuliporphyrins. Syntheses of ligands were conducted according to the general procedure described by Lash et al.[14]

**5,10,15,20-Tetraphenylazuliporphyrin-$d_x$ (1-$d_x$).** The deuterated ligand was obtained using a general procedure[14] with the appropriate modification to afford selective deuteration at $\beta$-positions. Prior to condensation chloroform stabilized with amylene was carefully dried over 4A molecular sieves. Azulene (160 mg, 1.25 mmol), pyrrole-$d_5$ (250 $\mu$L, 3.35 mmol), and benzaldehyde (460 $\mu$L, 4.45 mmol) were dissolved in freshly distilled dry, degassed chloroform (600 mL) in a 1 L round-bottomed flask equipped with stirring bar and a nitrogen inlet. $CH_3OD$ [6 mL, 1% (v/v)] was added to the reaction mixture. After that, boron trifluoride diethyl etherate (330 $\mu$L, 2.67 mmol) was added, and the mixture was stirred in the dark overnight (~17 h) under $N_2$. DDQ (800 mg, 3.52 mmol) was added, and the solution was stirred for further 60 min. Then the solvent was evaporated to dryness, and the residue was purified by chromatography on basic alumina (grade III) in gradient from dichloromethane/hexanes 1:2 to dichloromethane with small addition of $Et_3N$. The isolated product was deuterated in 85−90% on $\beta$-pyrrole hydrogen atoms as determined by $^1$H NMR.

**Carbonyl Ruthenium(II) 5,10,15,20-tetraaryl-21-oxyazuliporphyrin (3).** 5,10,15,20-tetraphenyl-21-hydroxyazuliporphyrin **1**−OH (5.0 mg, 7.23 $\mu$mol) was added to degassed benzene (20 mL) together with triruthenium(0) dodecacarbonyl (5.0 mg, 7.82 $\mu$mol). Mixture was refluxed for 1.5 h under nitrogen atmosphere. After solvent evaporation, the residue was subjected to purification on column chromatography (alumina, 6−8 (wt)% of water depending on $Al_2O_3$ activity, dichloromethane). After a residual orange fraction (of ruthenium carbonyl) at the beginning the pink fraction of unreacted ligand was collected. After changing eluent polarity to DCM: 1-butanol 50:1 (or using very diluted lower alcohols solutions) the red-pink narrow fraction of [Ru(TPAP-O)(CO)] was obtained (1.9 mg, 33%).

Reaction of **1**−OH (5.0 mg, 7.23 $\mu$mol) with triruthenium(0) dodecacarbonyl (5.0 mg, 7.82 $\mu$mol) conducted and worked up in analogous conditions resulted mainly in generation of **2** in 41% yield revealing the elimination of 21-oxy bridge. Larger amounts of $[Ru_3(CO)_{12}]$ used in the insertion afforded cluster [Ru(TPAP)(CO)-$\{Ru_4(CO)_9\}$].

**3** can be also collected as a minor product (a few percent) of **2** synthesis (ruthenium insertion to azuliporphyrin **1**) when solvent was not sufficiently degassed. Oxygenation of **2** conducted for 2 h in boiling chlorobenzene in aerobic conditions yielded 3% of **3** and recovery of unreacted **2** (after column chromatography).

**$^1$H NMR** (600 MHz, $CD_2Cl_2$ + Py-$d_5$, 300 K) $\delta$ 7.91 (d, $J$ = 6.5 Hz, 4H, 5,20-*o*Ph), 7.85 (d, $J$ = 5.1 Hz, 2H, 7,18), 7.83 (d, $J$ = 7.5 Hz, 2H, 10,15-*o*Ph), 7.63−7.58 (m, 6H, 5,20-*m*Ph, *p*Ph), 7.56 (td, $J$ = 7.5, 1.0 Hz, 2H, 10,15-*m*Ph), 7.50 (tt, $J$ = 7.5, 1.0 Hz, 2H, 10,15-*p*Ph), 7.43 (td, $J$ = 7.5, 1.0 Hz, 2H, 10,15-*m*Ph), 7.27 (d, $J$ = 5.1 Hz, 2H, 8,17), 7.27 (s, 2H, 12,13), 7.22 (d, $J$ = 7.5 Hz, 2H, 10,15-*o*Ph), 5.82 (dd, $J$ = 10.7, 9.4 Hz, 2H, $2^2$,$3^2$), 5.58 (t, $J$ = 9.4 Hz, 1H, $2^3$), 5.41 (d, $J$ = 10.7 Hz, 2H, $2^1$,$3^1$), **$^{13}$C NMR** (151 MHz, $CDCl_3$ + Py-$d_5$, 300 K) $\delta$ 182.0 (CO), 152.7, 151.9, 149.6, 143.3, 142.0, 141.1, 137.3, 136.6 ($2^2$,$3^2$), 135.6 (7,18), 135.2 (5,20-*o*Ph), 134.2 (12,13), 132.9 (10,15-*o*Ph), 132.8 (10,15-*o*Ph), 132.6, 129.6 ($2^1$,$3^1$), 128.9 ($2^3$), 128.1 (5,20-*p*Ph), 127.4 (10,15-*m*Ph), 127.2 (5,20-*m*Ph), 127.13 (10,15-*p*Ph), 127.09 (10,15-*m*Ph), 126.6 (8,17), 116.56, 116.53, **HRMS** (ESI) calcd for $C_{51}H_{31}N_3O_2Ru$ (M+H$^+$): 820.1538; found: 820.1521 ($m/z$) **IR** ($\nu_{CO}$) 1947 cm$^{-1}$, **UV−vis** (10% (v/v) $Et_3N/CHCl_3$) $\lambda_{max}$ (log $\varepsilon$) 389.0 (4.79), 524.6 (4.99), 648.6 (4.06), 679.7 (4.05) nm.

**Instrumentation.** NMR spectra were measured on Bruker Avance 500 MHz and Bruker Avance III 600 MHz spectrometers. $^1$H and $^{13}$C shifts were referenced to the residual resonances of deuterated solvents. The $^2$H NMR spectra were collected using a Bruker Avance 600 instrument operating at 92.12 MHz. Infrared absorption spectrum of **3** was measured on a Bruker FT-IR VERTEX70 spectrophotometer applying KBr disc. Experiment with DDQ was done by the ATR technique (thin films of **2** and **2** + DDQ (**6**) were measured). Absorption spectra were recorded on a Varian Carry-50 Bio spectrophotometer. Mass spectra (High Resolution and Accurate Mass) were recorded on a Bruker micrOTOF-Q spectrometer using the electrospray technique. EPR spectra were recorded on the Bruker ESP 300 spectrometer operating with an X-band equipped with an ER035Gmeter and a HP 53550B microwave frequency counter. Electrochemical measurements were performed with the EA9C Multifunctional Electrochemical Analyzer in following conditions: degassed, dry $CH_2Cl_2$, 0.1 M TBAP; scan rate 20 mV/s, working electrode−glassy carbon disk, auxiliary electrode−platinum wire, reference electrode—Ag/AgCl. The voltammograms were referenced against the half-wave potential of Fc/Fc$^+$.

**Crystallography.** The X-ray diffraction data for **3**-$^n$BuOH and **4** were collected on Oxford Diffraction Xcalibur with an Onyx detector (Cu K$\alpha$ radiation, $\lambda$ = 1.541 75 Å) and on Oxford Diffraction Xcalibur with a Ruby detector (Mo K$\alpha$ radiation; $\lambda$ = 0.710 73 Å), respectively. Single crystals suitable for the XRD experiment were obtained by cooling 1-butanol solution of [Ru(TPAP-O)(CO)] for **3**-$^n$BuOH and evaporating dichloromethane solution for **4**. The data for **3**-$^n$BuOH and **4** were collected at 100 K using an Oxford Cryosystem device. Data reduction and analysis were carried out with the CrysAlis "RED" program.[80] An analytical absorption correction was applied for



DOI: 10.1021/acs.inorgchem.5b00324
*Inorg. Chem.* 2015, 54, 6184−6194

**3**-$^n$BuOH. Space groups were determined using the XPREP program.[81] Structures were solved by direct methods using the SHELXS program and refined using all $F^2$ data, as implemented by the SHELXL program.[82] The SQUEEZE procedure[83] implemented into the PLATON program was applied for disordered noncoordinated solvent molecules, namely, 1-butanol (located in a special position) for **3**-$^n$BuOH and dichloromethane in **4**. Non-hydrogen atoms in **3**-$^n$BuOH and **4** were refined with anisotropic displacement parameters. All H atoms were found on $\Delta\rho$ maps or placed at calculated positions. Before the last cycle of refinement all H atoms were fixed and were allowed to ride on their parent atoms. Crystal data for **3**-$^n$BuOH: $C_{55}H_{41}N_3O_3Ru{\cdot}1.5C_4H_{10}O$, triclinic, $P\bar{1}$, $a$ = 13.666(3) Å, $b$ = 13.913(3) Å, $c$ = 14.580(4) Å, $\alpha$ = 73.20(2)°, $\beta$ = 67.95(3)°, $\gamma$ = 83.27(3)°, $V$ = 2459.6(12) Å$^3$, $T$ = 100(2) K, $R$ = 0.111, $wR$ = 0.2445 [2548 reflections with $I > 2\sigma(I)$] for 610 variables. Crystal data for **4**: $C_{102}H_{62}N_6O_4Ru_2{\cdot}CH_2Cl_2$, tetragonal, $P4_32_12$, $a$ = 13.427(3) Å, $c$ = 44.203(7) Å, $V$ = 7969(4) Å$^3$, $T$ = 100.02(10) K, $R$ = 0.106, $wR$ = 0.170 [1994 reflections with $I > 2\sigma(I)$] for 513 variables, Flack = −0.08(10).

**Density Functional Theory Calculations.** Geometry optimizations were performed within unconstrained $C_1$ symmetry in vacuo, with starting coordinates derived from preoptimized models using Gaussian software.[84] Calculations were performed using the spin-unrestricted approach (for open-shell models $\mathbf{6}_o$ and $\mathbf{7}_o$) with the B3LYP/6-31G(d,p) level of theory and pseudopotential (LANL2DZ) on Ru.[85,86] Harmonic frequencies were calculated using analytical second derivatives as a verification of local minimum achievement with no negative frequencies observed. Calculations of spin density were performed for the optimized models. Visualization of molecular orbitals and spin-density distribution was done with the use of GaussView program.[87]

## ■ ASSOCIATED CONTENT

### Supporting Information

NMR spectra ($^{13}$C NMR for **3**-py-$d_5$, $^1$H NMR of paramagnetic complexes **6**, variable-temperature $^1$H NMR experiment for **3**), HRMS for **3** and **4**, UV−vis (variable-temperature UV−vis studies of **3**, one-electron oxidation of [Ru(TPAP)(CO)] with DDQ), voltammetry measurements for **2** and **3**, EPR spectra of **6**-Br and **6**, DFT (models of $\mathbf{2}_o$-MeCN, $\mathbf{3}_o$-$H_2O$, $\mathbf{6}_o$, $\mathbf{6}_o$-Br, $\mathbf{7}_o$, distribution of the spin density on heavy atoms for $\mathbf{6}_o$ and $\mathbf{6}_o$-Br, diagram of molecular orbitals for $\mathbf{6}_o$-Br), crystal and structure refinement data for **3**-$^n$BuOH and **4**. This material is available free of charge via the Internet at http://pubs.acs.org.

## ■ AUTHOR INFORMATION


### Corresponding Author

*E-mail: lechoslaw.latos-grazynski@chem.uni.wroc.pl. Homepage: http://llg.chem.uni.wroc.pl/.


### Notes

The authors declare no competing financial interest.

## ■ ACKNOWLEDGMENTS


Financial support from the National Science Centre (Grant No. 2012/04/A/ST5/00593) is kindly acknowledged. DFT calculations were performed using resources provided by Wroclaw Centre for Networking and Supercomputing (http://wcss.pl), Grant No. 329. We thank Dr. L. Szterenberg for valuable discussions and Prof. P. Chmielewski and J. Zaręba for help in measurements.


## ■ REFERENCES


(1) Toganoh, M.; Furuta, H. Synthesis and Metal Coordination of N-Confused and N-Fused Porphyrinoids. In *Handbook of Porphyrin Science: with Applications to Chemistry, Physics, Materials Science, Engineering, Biology and Medicine;* Kadish, K. M., Smith, K. M., Guilard, R., Eds.; World Scientific Publishing: Singapore, 2010; pp 295−367.

(2) Pawlicki, M.; Latos-Grażyński, L. Carbaporphyrinoids—Synthesis and Coordination Properties. In *Handbook of Porphyrin Science: with Applications to Chemistry, Physics, Materials Science, Engineering, Biology and Medicine;* Kadish, K. M., Smith, K. M., Guilard, R., Eds.; World Scientific Publishing: Singapore, 2010; pp 104−192.

(3) Brückner, C.; Akhigbe, J.; Samankumara, L. P. Porphyrin Analogs Containing Non-Pyrrolic Heterocycles. In *Handbook of Porphyrin Science: With Applications to Chemistry, Physics, Materials Science, Engineering, Biology and Medicine;* Kadish, K. M., Smith, K. M., Guilard, R., Eds.; World Scientific Publishing: Singapore, 2014; pp 4−275.

(4) Lash, T. D. *Chem.—Asian. J.* **2014**, *9*, 682−705.

(5) Chmielewski, P. J.; Latos-Grażyński, L. *Coord. Chem. Rev.* **2005**, *249*, 2510−2533.

(6) Pacholska-Dudziak, E.; Latos-Grażyński, L. *Eur. J. Inorg. Chem.* **2007**, 2594−2608.

(7) Ishizuka, T.; Ikeda, S.; Toganoh, M.; Yoshida, I.; Ishikawa, Y.; Osuka, A.; Furuta, H. *Tetrahedron* **2008**, *64*, 4037−4050.

(8) Toganoh, M.; Furuta, H. *Chem. Commun.* **2012**, *48*, 937−954.

(9) Stępień, M.; Latos-Grażyński, L. *Acc. Chem. Res.* **2005**, *38*, 88−98.

(10) Pawlicki, M.; Kańska, I.; Latos-Grażyński, L. *Inorg. Chem.* **2007**, *46*, 6575−6584.

(11) Maeda, H.; Osuka, A.; Ishikawa, Y.; Aritome, I.; Hisaeda, Y.; Furuta, H. *Org. Lett.* **2003**, *5*, 1293.

(12) Grzegorzek, N.; Nojman, E.; Szterenberg, L.; Latos-Grażyński, L. *Inorg. Chem.* **2013**, *52*, 2599−2566.

(13) Lash, T. D.; Chaney, S. T. *Angew. Chem., Int. Ed. Engl.* **1997**, *36*, 839−840.

(14) Colby, D. A.; Lash, T. D. *Chem.—Eur. J.* **2002**, *8*, 5397−5402.

(15) Asao, T.; Ito, S.; Morita, N. *Tetrahedron Lett.* **1988**, *29*, 2839−2842.

(16) Colby, D. A.; Lash, T. D. *J. Org. Chem.* **2002**, *67*, 1031−1033.

(17) Sprutta, N.; Siczek, M.; Latos-Grażyński, L.; Pawlicki, M.; Szterenberg, L.; Lis, T. *J. Org. Chem.* **2007**, *72*, 9501−9509.

(18) Graham, S. R.; Ferrence, G. M.; Lash, T. D. *Chem. Commun.* **2002**, 894−895.

(19) Lash, T. D.; Colby, D. A.; Graham, S. R.; Ferrence, G. M.; Szczepura, L. F. *Inorg. Chem.* **2003**, *42*, 7326−7338.

(20) Lash, T. D.; Pokharel, K.; Zeller, M.; Ferrence, G. M. *Chem. Commun.* **2012**, *48*, 11793−11795.

(21) Berlicka, A.; Sprutta, N.; Latos-Grażyński, L. *Chem. Commun.* **2006**, 3346−3348.

(22) Colby, D. A.; Ferrence, G. M.; Lash, T. D. *Angew. Chem., Int. Ed.* **2004**, ASAP.

(23) Białek, M. J.; Latos-Grażyński, L. *Chem. Commun.* **2014**, *50*, 9270−9272.

(24) Walker, F. A. Proton NMR and EPR Spectroscopy of Paramagnetic Metalloporphyrins. In *The Porphyrin Handbook;* Kadish, K. M., Smith, K. M., Guilard, R., Eds.; Academic Press: San Diego, CA, 2000; pp 81−183.

(25) Bertini, I.; Luchinat, C. *Coord. Chem. Rev.* **1996**, *150*, 1.

(26) Bertini, I.; Luchinat, C.; Parigi, G. *Solution NMR of Paramagnetic Molecules, Application to Metallobiomolecules and Models.* In *Current Methods in Inorganic Chemistry,* 2001 ed.; Elsevier: Amsterdam, 2001.

(27) Walker, F. A. NMR and EPR Spectroscopy of Paramagnetic Metalloporphyrin and Heme Proteins. In *Handbook of Porphyrin Science: with Applications to Chemistry, Physics, Materials Science, Engineering, Biology and Medicine;* Kadish, K. M., Smith, K. M., Guilard, R., Eds.; World Scientific Publishing: Singapore, 2010; pp 1−337.

(28) Myśliborski, R.; Rachlewicz, K.; Latos-Grażyński, L. *Inorg. Chem.* **2006**, *45*, 7828−7834.

(29) Myśliborski, R.; Rachlewicz, K.; Latos-Grażyński, L. *J. Porphyrins Phtalocyanines* **2007**, *11*, 172−180.

(30) Rachlewicz, K.; Wang, S. L.; Peng, C. H.; Hung, C. H.; Latos-Grażyński, L. *Inorg. Chem.* **2003**, *42*, 7348−7350.

(31) Rachlewicz, K.; Wang, S. L.; Ko, J. L.; Hung, C. H.; Latos-Grażyński, L. *J. Am. Chem. Soc.* **2004**, *126*, 4420−4431.




DOI: 10.1021/acs.inorgchem.5b00324
*Inorg. Chem.* 2015, 54, 6184−6194

(32) Rachlewicz, K.; Gorzelańczyk, D.; Latos-Grażyński, L. *Inorg. Chem.* **2006**, *45*, 9742−9747.
(33) Berlicka, A.; Latos-Grażyński, L. *Inorg. Chem.* **2009**, *48*, 7922−7930.
(34) Chmielewski, P. J.; Latos-Grażyński, L.; Głowiak, T. *J. Am. Chem. Soc.* **1996**, *118*, 5690−5701.
(35) Chmielewski, P. J.; Latos-Grażyński, L.; Schmidt, I. *Inorg. Chem.* **2000**, *39*, 5475−5482.
(36) Pacholska-Dudziak, E.; Gaworek, A.; Latos-Grażyński, L. *Inorg. Chem.* **2011**, *50*, 10956−10965.
(37) Hung, C. H.; Chang, F. C.; Lin, C. Y.; Rachlewicz, K.; Stępień, M.; Latos-Grażyński, L.; Lee, G. H.; Peng, S. M. *Inorg. Chem.* **2004**, *43*, 4118−4120.
(38) Stępień, M.; Latos-Grażyński, L.; Szterenberg, L.; Panek, J.; Latajka, Z. *J. Am. Chem. Soc.* **2004**, *126*, 4566−4580.
(39) Guilard, R.; van Caemelbecke, E.; Tabard, A.; Kadish, K. M. Synthesis, Spectroscopy and Electrochemical Properties of Porphyrins with Metal-Carbon. In *The Porphyrin Handbook;* Kadish, K. M., Smith, K. M., Guilard, R., Eds.; Academic Press: San Diego, CA, 2000; pp 295−345.
(40) Sanders, J. K. M.; Bampos, N.; Clyde-Watson, Z.; Darling, S. L.; Hawley, J. C.; Kim, H. J.; Mak, C. C.; Webb, S. J. Axial Coordination Chemistry of Metalloporphyrins. In *The Porphyrin Handbook;* Kadish, K. M., Smith, K. M., Guilard, R., Eds.; Academic Press: San Diego, CA, 2000; pp 1−48.
(41) Gianferrara, T.; Bratsos, I.; Iengo, E.; Milani, B.; Ostric, A.; Spagnul, C.; Zangrando, E.; Alessio, E. *Dalton Trans.* **2009**, 10742−10756.
(42) Beletskaya, I.; Tyurin, V. S.; Tsivadze, A. Y.; Guilard, R.; Stern, C. *Chem. Rev.* **2009**, *109*, 1659−1713.
(43) Che, C. M.; Ho, C. M.; Huang, J. S. *Coord. Chem. Rev.* **2007**, *251*, 2145−2166.
(44) Lu, H.; Zhang, X. *Chem. Soc. Rev.* **2011**, *40*, 1899−1909.
(45) Bonnet, J. J.; Eaton, S. S.; Eaton, G. R.; Holm, R. H.; Ibers, J. A. *J. Am. Chem. Soc.* **1973**, *95*, 2141−2149.
(46) Salzmann, R.; Ziegler, C. J.; Godbout, N.; McMahon, M. T.; Suslick, K. S.; Oldfield, E. *J. Am. Chem. Soc.* **1998**, *120*, 11323−11334.
(47) Eaton, S. S.; Eaton, G. R. *Inorg. Chem.* **1976**, *15*, 134−139.
(48) Hung, C. H.; Chen, W. C.; Lee, G. H.; Peng, S. M. *Chem. Commun.* **2002**, 1516−1517.
(49) Xiao, Z. W.; Patrick, B. O.; Dolphin, D. *Inorg. Chem.* **2003**, *42*, 8125−8127.
(50) Lin, W. C.; Hsaio, D. Z.; Chang, W. P.; Chen, J. H.; Wang, S. S.; Tung, J. Y. *Polyhedron* **2012**, *42*, 243−248.
(51) Hanson, S. K.; Heinekey, D.; Goldberg, K. I. *Organometallics* **2008**, *27*, 1454−1463.
(52) Morishima, I.; Shiro, Y.; Takamuki, Y. *J. Am. Chem. Soc.* **1983**, *105*, 6168−6170.
(53) Morishima, I.; Shiro, Y.; Nakajima, K. *Biochemistry* **1986**, *25*, 3576−3584.
(54) Rachlewicz, K.; Latos-Grażyński, L. *Inorg. Chim. Acta* **1988**, *144*, 213−216.
(55) Rachlewicz, K.; Grzeszczuk, M.; Latos-Grażyński, L. *Polyhedron* **1993**, *12*, 821−829.
(56) Cheng, R. J.; Lin, S. H.; Mo, H. M. *Organometallics* **1997**, *16*, 2121−2126.
(57) Galardon, E.; Le Maux, P.; Paul, C.; Poriel, C.; Simonneaux, G. *J. Organomet. Chem.* **2001**, *629*, 145−152.
(58) Mu, X. H.; Kadish, K. M. *Langmuir* **1990**, *6*, 51−56.
(59) Kadish, K. M.; Tagliatesta, P.; Hu, Y.; Deng, Y. J.; Mu, X. H.; Bao, L. Y. *Inorg. Chem.* **1991**, *30*, 3737−3743.
(60) Ke, M.; Sishta, C.; James, B. R.; Dolphin, D.; Sparapany, J. W.; Ibers, J. A. *Inorg. Chem.* **1991**, *30*, 4766−4771.
(61) Latos-Grażyński, L.; Lisowski, J.; Chmielewski, P. J.; Grzeszczuk, M.; Olmstead, M. M.; Balch, A. L. *Inorg. Chem.* **1994**, *33*, 192−197.
(62) Nardis, S.; Cicero, D. O.; Licoccia, S.; Pomarico, G.; Berna, B. B.; Sette, M.; Ricciardi, G.; Rosa, A.; Fronczek, F. R.; Smith, K. M.; Paolesse, R. *Inorg. Chem.* **2014**, *53*, 4215−4227.
(63) Ikeue, T.; Ohgo, Y.; Saitoh, T.; Nakamura, M.; Fujii, H.; Yokoyama, M. *J. Am. Chem. Soc.* **2000**, *122*, 4068−4076.
(64) Nakamura, M. *Coord. Chem. Rev.* **2006**, *250*, 2271−2294.
(65) Ghosh, A.; Gonzalez, E.; Vangberg, T. *J. Phys. Chem. B* **1999**, *103*, 1363−1367.
(66) Hirao, H.; Shaik, S.; Kozlowski, P. M. *J. Phys. Chem. A* **2006**, *110*, 6091−6099.
(67) Ghosh, A.; Steene, E. *J. Biol. Chem.* **2001**, *6*, 739−752.
(68) Vangberg, T.; Lie, R.; Ghosh, A. *J. Am. Chem. Soc.* **2002**, *124*, 8122−8130.
(69) Szterenberg, L.; Latos-Grażyński, L.; Wojaczyński, J. *ChemPhysChem* **2002**, *3*, 575−583.
(70) Shokhirev, N. V.; Walker, F. A. *J. Phys. Chem.* **1995**, *99*, 17795−17804.
(71) Szterenberg, L.; Latos-Grażyński, L.; Wojaczyński, J. *ChemPhysChem* **2003**, *4*, 691−698.
(72) Seyler, J. W.; Fanwick, P. E.; Leidner, C. R. *Inorg. Chem.* **1990**, *29*, 2021.
(73) Seyler, J. W.; Safford, L. K.; Fanwick, P. E.; Leidner, C. R. *Inorg. Chem.* **1992**, *31*, 1545.
(74) Brothers, P. J.; Collman, J. P. *Acc. Chem. Res.* **1986**, *19*, 209−215.
(75) Collman, J. P.; Brothers, P. J.; Mcelweewhite, L.; Rose, E.; Wright, L. J. *J. Am. Chem. Soc.* **1985**, *107*, 4570−4571.
(76) Kohl, S. W.; Weiner, L.; Schwartsburd, L.; Konstantinovski, L.; Shimon, L. J.; Ben-David, Y.; Iron, M. A.; Milstein, D. *Science* **2009**, *324*, 74−77.
(77) van der Boom, M. E.; Milstein, D. *Chem. Rev.* **2003**, *103*, 1759−1792.
(78) Gunanathan, C.; Milstein, D. *Acc. Chem. Res.* **2011**, *44*, 588−602.
(79) Gagliardo, M.; Snelders, D. J.; Chase, P. A.; Gebbink, R. J.; van Klink, G. R.; van Koten, G. *Angew. Chem., Int. Ed.* **2007**, *46*, 8558−8573.
(80) *CrysAlis RED;* Oxford Diffraction: Wrocław, Poland, 2001.
(81) *Data Preparation & Reciprocal Space Exploration, Ver. 5.1/NT;* Bruker Analytical X-ray Systems: Kalrsruhe, Germany, 1997.
(82) Sheldrick, G. M. *Acta Crystallogr., Sect. A: Found. Crystallogr.* **2008**, *64*, 112−122.
(83) Spek, A. L. *Acta Crystallogr., Sect D: Biol. Crystallogr.* **2009**, *65*, 148−155.
(84) Frisch, M. J.; Trucks, G. W.; Schlegel, H. B.; Scuseria, G. E.; Robb, M. A.; Cheeseman, J. R.; Scalmani, G.; Barone, V.; Mennucci, B.; Petersson, G. A.; Nakatsuji, H.; Caricato, M.; Li, X.; Hratchian, H. P.; Izmaylov, A. F.; Bloino, J.; Zheng, G.; Sonnenberg, J. L.; Hada, M.; Ehara, M.; Toyota, K.; Fukuda, R.; Hasegawa, J.; Ishida, M.; Nakajima, T.; Honda, Y.; Kitao, O.; Nakai, H.; Vreven, T.; Montgomery, J. A., Jr.; Peralta, J. E.; Ogliaro, F.; Bearpark, M.; Heyd, J. J.; Brothers, E.; Kudin, K. N.; Staroverov, V. N.; Kobayashi, R.; Normand, J.; Raghavachari, K.; Rendell, A.; Burant, J. C.; Iyengar, S. S.; Tomasi, J.; Cossi, M.; Rega, N.; Millam, N. J.; Klene, M.; Knox, J. E.; Cross, J. B.; Bakken,V.; Adamo, C.; Jaramillo, J.; Gomperts, R.; Stratmann, R. E.; Yazyev, O.; Austin, A. J.; Cammi, R.; Pomelli, C.; Ochterski, J. W.; Martin, R. L.; Morokuma, K.; Zakrzewski, V. G.; Voth, G. A.; Salvador, P.; Dannenberg, J. J.; Dapprich, S.; Daniels, A. D.; Farkas, Ö.; Foresman, J. B.; Ortiz, J. V.; Cioslowski, J.; Fox, D. J. *Gaussian 09, Revision D.01;* Gaussian, Inc.: Wallingford, CT, 2009.
(85) Lee, C.; Yang, W.; Parr, R. G. *Phys. Rev. B* **1988**, *37*, 785−789.
(86) Becke, A. D. *Phys. Rev. A* **1988**, *38*, 3098−3100.
(87) Dennington, R.; Keith, T.; Millam, J. *GaussView, Version 5;* Semichem Inc.: Shawnee Mission, KS, 2009.


DOI: 10.1021/acs.inorgchem.5b00324
*Inorg. Chem.* 2015, 54, 6184−6194